

# Accelerating Stochastic Gravitational Wave Backgrounds Parameter Estimation in Pulsar Timing Arrays with Flow Matching

Bo Liang,<sup>1,2,3,\*</sup> Chang Liu,<sup>1,4,\*</sup> Tianyu Zhao,<sup>1,†</sup> Minghui Du,<sup>1</sup> Manjia Liang,<sup>1</sup> Ruijun Shi,<sup>5,6</sup> Hong Guo,<sup>7</sup> Yuxiang Xu,<sup>1,2,3</sup> Li-e Qiang,<sup>1,4</sup> Peng Xu,<sup>1,8,3,9,‡</sup> Wei-Liang Qian,<sup>7</sup> and Ziren Luo<sup>1,8,3</sup>

<sup>1</sup>*Center for Gravitational Wave Experiment, National Microgravity Laboratory,  
Institute of Mechanics, Chinese Academy of Sciences, Beijing 100190, China*

<sup>2</sup>*Shanghai Institute of Optics and Fine Mechanics,  
Chinese Academy of Sciences, Shanghai 201800, China*

<sup>3</sup>*Taiji Laboratory for Gravitational Wave Universe (Beijing/Hangzhou),  
University of Chinese Academy of Sciences (UCAS), Beijing 100049, China*

<sup>4</sup>*National Space Science Center, Chinese Academy of Sciences, Beijing 100190, China*

<sup>5</sup>*School of Physics and Astronomy, Beijing Normal University, Beijing, 100875, China*

<sup>6</sup>*Institute for Frontiers in Astronomy and Astrophysics,  
Beijing Normal University, Beijing, 102206, China*

<sup>7</sup>*Escola de Engenharia de Lorena, Universidade de São Paulo, 12602-810, Lorena, SP, Brazil*

<sup>8</sup>*Key Laboratory of Gravitational Wave Precision Measurement of Zhejiang Province,  
Hangzhou Institute for Advanced Study, UCAS, Hangzhou 310024, China*

<sup>9</sup>*Lanzhou Center of Theoretical Physics, Lanzhou University, Lanzhou 730000, China*

Pulsar timing arrays (PTAs) are essential tools for detecting the stochastic gravitational wave background (SGWB), but their analysis faces significant computational challenges. Traditional methods like Markov-chain Monte Carlo (MCMC) struggle with high-dimensional parameter spaces where noise parameters often dominate, while existing deep learning approaches fail to model the Hellings-Downs (HD) correlation or are validated only on synthetic datasets. We propose a flow-matching-based continuous normalizing flow (CNF) for efficient and accurate PTA parameter estimation. By focusing on the 10 most contributive pulsars from the NANOGrav 15-year dataset, our method achieves posteriors consistent with MCMC, with a Jensen-Shannon divergence below  $10^{-2}$  nat, while reducing sampling time from 50 hours to 4 minutes. Powered by a versatile embedding network and a reweighting loss function, our approach prioritizes the SGWB parameters and scales effectively for future datasets. It enables precise reconstruction of SGWB and opens new avenues for exploring vast observational data and uncovering potential new physics, offering a transformative tool for advancing gravitational wave astronomy.

**Introduction.**— Pulsar timing arrays (PTAs) have emerged as a crucial tool in astrophysics, offering unique insights into the cosmos. Recent observations from various collaborations, including the NanoGrav [1, 2], European pulsar timing array (EPTA) [3], Parks pulsar timing array (PPTA) [4], and Chinese pulsar timing array (CPTA) [5], have confirmed the existence of stochastic gravitational wave background (SGWB) [6, 7]. This groundbreaking achievement highlights the potential of PTAs to probe the fabric of spacetime, enriching our understanding of the evolutions of supermassive black holes and other cosmological phenomena [8]. Such capabilities provide a promising avenue for unraveling mysteries that lie beyond the reach of traditional observational methods [9].

Despite these advancements, traditional data analysis methods—particularly Markov-chain Monte Carlo (MCMC) techniques—face significant challenges in parameter estimation for PTAs [10–13]. The high dimensionality of the parameter space and the extended data length increase the challenges of both time-domain and

frequency-domain analyses [14]. MCMC methods are often hindered by slow convergence and require extensive computational resources, rendering them inefficient when confronted with the increasingly complex datasets produced by modern PTAs [15, 16]. Moreover, intricate interdependencies among parameters can lead to degeneracy [17], resulting in biased estimates and significantly increased computational costs. As PTAs datasets continue to grow in size and complexity, these limitations underscore the urgent need for more efficient and robust estimation techniques [18].

Artificial intelligence is revolutionizing scientific data analysis, particularly in the context of parameter estimation (PE) for PTA studies and gravitational wave (GW) detection, as seen with [Laser Interferometer Gravitational Wave Observatory \(LIGO\)](#) and [Laser Interferometer Space Antenna \(LISA\)](#) [19–21]. Deep learning has shown promise in enhancing data analysis capabilities; however, existing approaches, such as neural parameter estimation (NPE) [22–24], often fall short due to the still slower processing times and potential inaccuracies. These limitations become particularly evident when applied to real observational scenarios in PTA data analysis and SGWB detection, where the intricate nature of signals demands more sophisticated techniques [25]. Previous studies had applied NPE or related methods to PTA

\* These authors contributed equally to the work.

† zhaotianyu@imech.ac.cn

‡ xupeng@imech.ac.cn

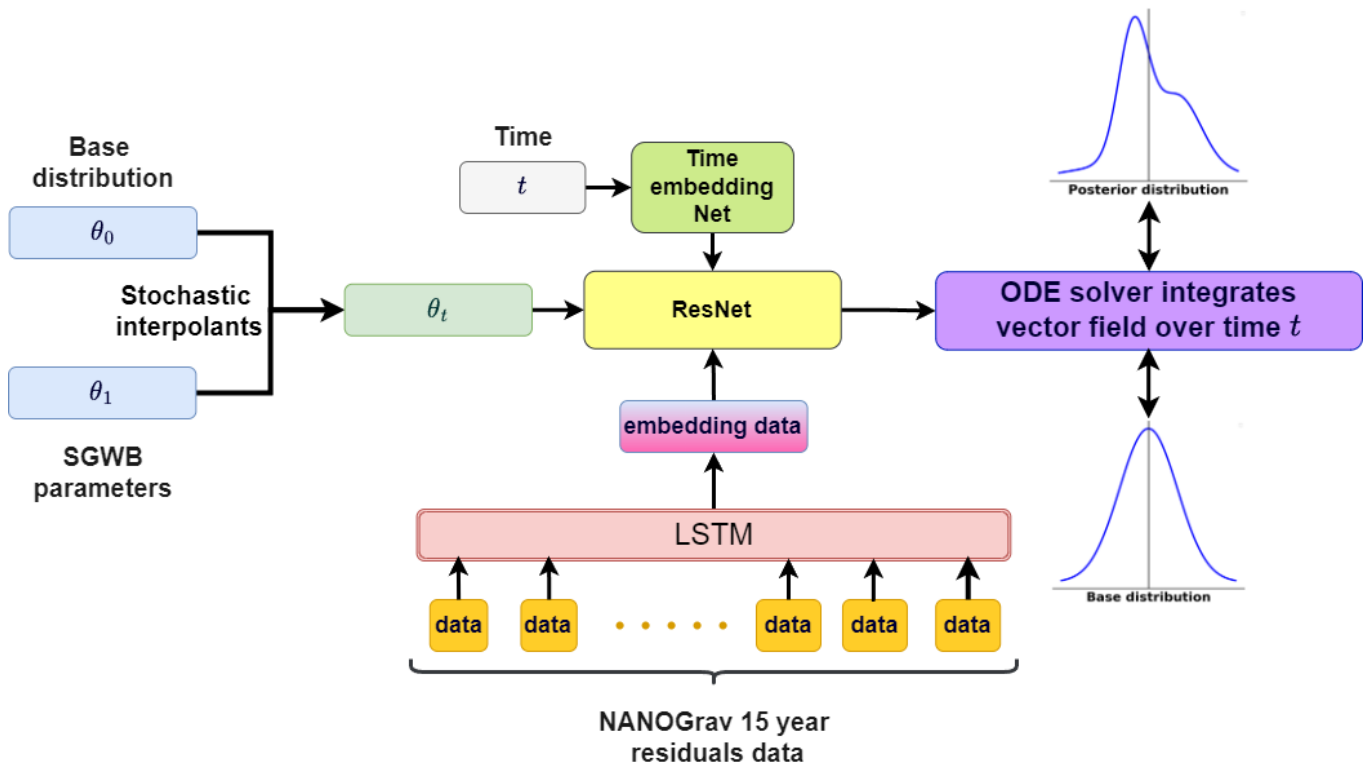


Figure 1. The figure illustrates the framework for training using CNFs.  $t$  represents the sampling time, with a range from 0 to 1. In describing the transition from the initial Gaussian distribution  $\theta_0$  to the SGWB posterior distribution  $\theta_1$ , we use linear interpolation to construct the distribution  $\theta_t$  at any given time  $t$ . Additionally, we utilize LSTM to construct an embedding network, aimed at processing NG15 real PTA residual data related to the power-law spectrum of HD. Once CNFs are trained, they can use an ODE solver to transform the initial base distribution into posterior distribution. This process involves utilizing the invertible property of CNFs to solve a mapping obtained from a neural ordinary differential equation (ODE), thereby achieving a transition from a simple distribution to a complex one.

data and SGWB detection [26, 27]; however, these works had limitations: they only worked with synthetic data or were restricted to the analysis of common uncorrelated red noise (CURN) parameters only, without capturing the full Hellings-Downs (HD) correlation characteristic of SGWB signals [28].

We introduce a novel flow-matching-based continuous normalizing flow (CNF) method for parameter estimation in PTA data [21, 25, 29, 30]. Utilizing recent advancements in flow-matching techniques [21, 25, 31], our approach efficiently trains on just 10 pulsars out of 68, greatly enhancing training efficiency [32]. Applying our method to the NANOGrav 15-year dataset [6], we perform posterior estimation on real data characterized by the HD correlated power-law spectrum of the SGWB [28]. Our results demonstrate that the obtained posterior distributions are consistent with those from MCMC analyses [12, 13, 33], while significantly reducing computation time. Remarkably, our model can generate the posterior distributions within 30 seconds through model inference. We believe this advancement not only accelerates SGWB parameter estimation but also has the potential to revolutionize future PTA data analysis pipelines. We hope this work will encourage broader adoption of these innovative

methods in experimental science, particularly in PTA analysis and SGWB parameter estimation.

**Dataset Generation.**— In constructing our simulated pulsar timing dataset, our goal is to accurately model the key sources of signals and noise relevant to our parameter estimation method. Based on the 15 years of NANOGrav data [6], we generated 1.5 million pulsar timing residual time series. We focused on ten pulsars that provide the most compelling evidence for an isotropic SGWB signal in the NANOGrav datasets [32], as detailed in Tab. I. This extensive dataset forms the foundation for training and validating our CNF model.

Table I. The ten pulsars providing the strongest evidence for SGWB and their high dropout factors [32]

Pulsar	Dropout Factor	Pulsar	Dropout Factor
J1909–3744	17.6	J0030+0451	2.4
J2317+1439	14.5	J1910+1256	2.4
J2043+1711	6.0	J1744–1134	2.5
J1600–3053	5.3	J1944+0907	3.3
J1918–0612	3.4	J0613–0200	3.4

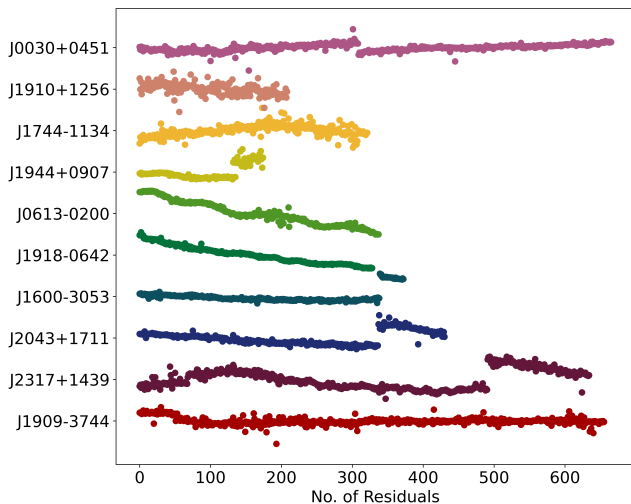


Figure 2. We selected real residual data from ten pulsars in NANOGrav15 for analysis. These pulsars provided the strongest evidence for a SGWB in NANOGrav12.5, providing a solid data foundation for our research.

The SGWB signal is modeled as a common process affecting all pulsars, characterized by an amplitude  $A_{\text{GW}}$  and a spectral index  $\gamma_{\text{GW}}$ . The power spectral density (PSD) of the SGWB-induced timing residuals follows a power-law spectrum given by

$$P_{\text{SGWB}}(f) = \frac{A_{\text{GW}}^2}{12\pi^2} \left( \frac{f}{f_{\text{ref}}} \right)^{-\gamma_{\text{GW}}} f_{\text{ref}}^{-3}, \quad (1)$$

where  $f$  is the frequency and  $f_{\text{ref}} = 1 \text{ yr}^{-1}$  is the reference frequency. To capture the spatial correlations between pulsars due to the SGWB, we incorporated the HD-correlation matrix  $\chi_{IJ}$ , defined by

$$\chi_{IJ} = \frac{3}{2} \left[ \left( \frac{1 - \cos \theta_{IJ}}{2} \right) \ln \left( \frac{1 - \cos \theta_{IJ}}{2} \right) - \frac{1}{6} (1 - \cos \theta_{IJ}) + \frac{1}{3} \right], \quad (2)$$

where  $\theta_{IJ}$  is the angular separation between pulsars  $I$  and  $J$ . We simulated  $\chi_{IJ}$  by calculating the angular separations between the ten selected pulsars and evaluating the HD function for each pair. Each pulsar also has its own intrinsic red noise, with amplitude  $A_r^{(i)}$  and spectral index  $\gamma_r^{(i)}$ , following a similar power-law spectrum:

$$P_{\text{red}}^{(i)}(f) = \frac{A_r^{(i)2}}{12\pi^2} \left( \frac{f}{f_{\text{ref}}} \right)^{-\gamma_r^{(i)}} f_{\text{ref}}^{-3}. \quad (3)$$

In order to better fit the real situation, we have individually processed the white noise level  $\sigma$  for each pulsar, and set  $\sigma = \sigma_i$  where  $\sigma_i$  is a specific value obtained for each selected pulsar after processing the NG15 data with the ENTERPRISE software, and the average level of these values is roughly between 100-500 ns.

This approach allowed us to accurately simulate both the common SGWB signal—including its HD correlations—and the individual noise characteristics of each pulsar.

Before training, we pre-processed the simulated residuals to optimize the performance of our machine learning model. This involved rescaling the residuals to ensure that they were within a suitable range for neural network training. The ten pulsars contribute a total of 4,944 projected residuals, providing a rich dataset for analysis. We partitioned the 1.5 million generated time series into two sets: 98% were used for training the CNFs, and the remaining 2% were reserved for model validation. This dataset enabled us to effectively train and validate our model.

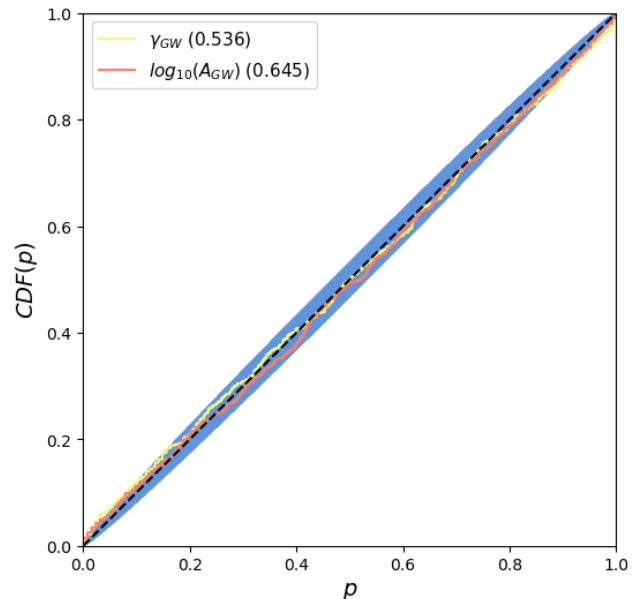


Figure 3. In the P-P plot of 800 injections, the p-values for each parameter are indicated in the legend, and the average p-value across all parameters is calculated to be 0.591.

**Model Architecture.**— In this Letter, we employ CNF to fit the posterior distribution of the NANOGrav15 dataset [6], modeling it with a power-law spectrum and incorporating HD correlations. To optimize the CNFs, we utilize flow matching [21, 25, 30], a novel technique in artificial intelligence that accelerates the training of CNFs. This method, known as flow-matching parameter estimation (FMPE), enhances efficiency and precision in modeling complex distributions.

A CNF defines a transformation of a probability density through a continuous-time dynamical system. Given a base distribution  $p_0(\boldsymbol{\theta}_0)$  and a target distribution  $p_1(\boldsymbol{\theta}_1)$ , the transformation is defined by the ordinary differential equation (ODE) [29]:

$$\frac{d}{dt} \psi_{t,x}(\boldsymbol{\theta}) = v_{t,x}(\psi_{t,x}(\boldsymbol{\theta})). \quad (4)$$

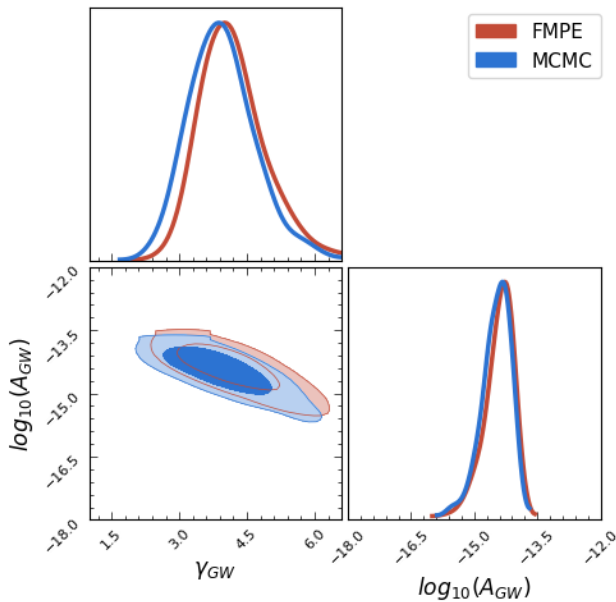


Figure 4. In estimating the parameters of the power-law spectrum SGWB associated with HD, CNFs show a significant speed advantage. The method can complete parameter estimation in tens of seconds (indicated in blue), which matches the results provided by Enterprise (indicated in orange) and is several orders of magnitude faster than existing methods.

Where,  $\psi_{t,x}(\boldsymbol{\theta})$  describes the transition from the base distribution  $p_0(\boldsymbol{\theta}_0)$  to the target distribution  $p_1(\boldsymbol{\theta}_1)$ .

To train the CNF, we employ the flow-matching loss function [30, 34], which minimizes the difference between the vector field  $v_{t,x}(\psi_{t,x}(\boldsymbol{\theta}))$  and the optimal vector field  $u_t(\boldsymbol{\theta}|\boldsymbol{\theta}_1)$  that transports  $p_0$  to  $p_1$ . The flow-matching loss is given by:

$$\mathcal{L}_{\text{FM}} = \mathbb{E}_{t \sim p(t)} \mathbb{E}_{\boldsymbol{\theta}_1 \sim p(\boldsymbol{\theta})} \mathbb{E}_{x \sim p(x|\boldsymbol{\theta}_1)} \mathbb{E}_{\boldsymbol{\theta}_t \sim p_t(\boldsymbol{\theta}_t|\boldsymbol{\theta}_1)} \| r \|^2. \quad (5)$$

Where  $p(\boldsymbol{\theta})$  is the logit normal sampling strategy [35], with  $m = 0, s = 1$ . Where  $r$  is the residual vector field:

$$r = v_{t,x}(\boldsymbol{\theta}_t) - u_t(\boldsymbol{\theta}_t|\boldsymbol{\theta}_1) \quad (6)$$

Different from flow matching, in this work we are inspired by stable diffusion 3 [35]. We define the  $p_t(\boldsymbol{\theta}|\boldsymbol{\theta}_1)$  as:

$$p_t(\boldsymbol{\theta}|\boldsymbol{\theta}_1) = \mathcal{N}(t\boldsymbol{\theta}_1, 1 - t). \quad (7)$$

Thus the optimal vector field  $u_t(\boldsymbol{\theta}|\boldsymbol{\theta}_1)$  is defined as [36, 37]:

$$u_t(\boldsymbol{\theta}|\boldsymbol{\theta}_1) = \boldsymbol{\theta}_1 - \boldsymbol{\theta}_0. \quad (8)$$

In practice,  ${}_t\boldsymbol{\theta}_t|\boldsymbol{\theta}_1$  can be approximated by sampling from the conditional distribution  $p(\boldsymbol{\theta}_1|\boldsymbol{\theta}_t)$ .

In PTA research, a key challenge lies in effectively addressing the high-dimensional noise parameters, which can span tens of dimensions, compared to the two-dimensional

SGWB parameters associated with the HD correlation. The dominance of noise parameter dimensions often limits the focus on SGWB signals, leading to high computational costs and convergence difficulties in MCMC analysis. To tackle these challenges, we introduce a hyperparameter  $\lambda$  into the loss function, defined as:

$$\mathcal{L} = \lambda \cdot \mathcal{L}_{\text{FM}}^{\text{SGWB}} + (1 - \lambda) \cdot \mathcal{L}_{\text{FM}}^{\text{Noise}}. \quad (9)$$

This approach enables flexible reweighting of the model’s attention, allowing it to prioritize the fitting of the SGWB. By balancing the contributions of SGWB and noise parameters, our method improves both the efficiency and accuracy of parameter estimation.

Our model architecture comprises two main components, as illustrated in Fig. 1. The **first component** is an embedding network designed to process the 4,944 residuals from the ten pulsars and perform feature extraction. Since our flow network ultimately fits a two-dimensional vector field, the embedding network is essential for reducing the high-dimensional input data to a manageable size. We employ a long short-term memory (LSTM) network as the embedding network [38], which compresses the features of each pulsar into 100 dimensions. These features are further refined and compressed into 50 dimensions using a residual network [39]. The resulting compressed features, denoted as  $\mathbf{c} \in \mathbb{R}^{50}$ , serve as conditional inputs to the flow network.

The **second component** is the flow network itself, consisting of 56 residual blocks with gradually decreasing sizes. The vector field  $\mathbf{v}_{t,x}(\boldsymbol{\theta}_t)$  is parameterized by the neural network  $f_{\boldsymbol{\theta}}$  and conditioned on the embedded features  $\mathbf{c}$  and the time parameter  $t$ . Specifically, the flow network takes as input the triplet  $(\boldsymbol{\theta}_t, t, \mathbf{c})$  and outputs the vector field:

$$\mathbf{v}_{t,x}(\boldsymbol{\theta}_t) = f_{\boldsymbol{\theta}}(\boldsymbol{\theta}_t, t, \mathbf{c}). \quad (10)$$

To implement our normalized flow and embedding networks, we chose the PyTorch [40] framework combined with the numpy [41] library, as well as the zuko [42] and lampe [43] software packages. The model was trained for 100 epochs utilizing a batch size of 512, employing the Adam optimizer [44] for efficient convergence. The initial learning rate was set to 0.0001 and was gradually reduced to zero using a cosine annealing schedule. Training was conducted on an NVIDIA RTX 4090 GPU and took approximately 20 hours. Remarkably, sampling from the trained CNF to produce posterior distributions involves solving the ODE, which takes approximately 240 seconds for 8,192 samples using a Runge-Kutta solver [45, 46]. In contrast, generating an equivalent number of posterior draws using the traditional MCMC pipeline takes approximately 50 hours on an Apple M3 Max chip. This significant reduction in computation time demonstrates the efficiency and practicality of our approach for large-scale PTA data analysis.

**Results.**— We apply our method to the NANOGrav 15 years dataset (Fig. 2) to estimate the parameters of

Table II. This table compares the parameters recovered by the FMPE and MCMC methods. The recovered values are accompanied by their  $1\sigma$  confidence regions. The last column of the table presents the JS divergence between the FMPE and MCMC marginalised posteriors

	FMPE	MCMC	JS divergence [ $10^{-2}$ nat]
$\gamma_{\text{GW}}$	$3.91^{+0.72}_{-0.62}$	$4.11^{+0.78}_{-0.58}$	0.67
$A_{\text{GW}}$	$-14.45^{+0.28}_{-0.37}$	$-14.36^{+0.26}_{-0.39}$	0.01

a SGWB incorporating HD-correlations. Fig. 4 presents a corner plot comparing the posterior distributions obtained from our flow-matching-based CNF model with those from a traditional MCMC analysis. The CNF-generated posteriors closely align with the MCMC results, accurately capturing the intricate correlations between the SGWB amplitude  $A_{\text{GW}}$  and spectral index  $\gamma_{\text{GW}}$ . As shown in Tab. II, the Jensen-Shannon (JS) divergence between our method and MCMC results is below  $10^{-2}$  nat, highlighting the exceptional fidelity of our approach. This demonstrates that our method not only matches the accuracy of established techniques but also surpasses previous deep learning approaches in precision and efficiency. For instance, Shih *et al.* [26] employed NPE on 12.5-year synthetic data, whereas our work successfully handles real observational data from the 15-year dataset using a flow-matching-based CNF. Additionally, unlike the approach by Vallisneri *et al.* [27], which is restricted to analyzing common uncorrelated red noise (CURN) parameters without capturing the full HD correlation characteristic of SGWB signals, our method fully accounts for these correlations. Remarkably, our CNF method accomplishes this comprehensive analysis with a substantial reduction in computational time—from approximately 50 hours for MCMC to merely 4 minutes for CNF sampling—demonstrating its high efficiency and scalability for large datasets.

To evaluate the unbiasedness of our parameter estimation, we perform a cumulative distribution function p-p plot analysis, as depicted in Fig. 3. This plot compares the cumulative distribution functions of the estimated parameters against the uniform distribution expected from perfectly unbiased estimators. Our results adhere closely to the diagonal line, indicating that the CNF model produces unbiased estimates of the SGWB parameters across multiple data realizations. By effectively handling real data and capturing the full HD correlations—overcoming the limitations of previous studies that used NPE methods—our flow-matching-based CNF approach underscores the potential of advanced machine learning techniques to revolutionize PTA data analysis. Our method offers

a viable and alternative to traditional MCMC methods for current and future datasets, efficiently addressing the complexities and computational demands that have challenged past methodologies.

As the PTA dataset grows increasingly large, the spectral constraints on SGWB will become more precise due to the expansion of the dataset, which will help reveal its origins. At the same time, future PTA observations will deepen our understanding of this signal and its astrophysical and cosmological interpretations. However, with the growth of the dataset, traditional MCMC-based techniques face the challenge of exponential growth in computational time. Machine learning techniques offer a promising alternative, with the potential to enhance parameter estimation for PTA data and complement existing MCMC methods. These advancements will enable more efficient analysis of larger and more complex PTA datasets, paving the way for precise reconstructions of gravitational wave backgrounds and uncovering potential new physics.

**Discussion.**— In this study, we introduced CNFs as a highly expressive technique for parameter estimation in PTA data analysis. While CNFs have demonstrated remarkable capabilities in handling PTA data, their performance is currently limited by the variable sequence lengths inherent in pulsar timing residuals. This limitation arises because traditional embedding networks struggle to effectively process sequences of varying lengths, potentially hindering the model’s ability to capture all relevant temporal features. To overcome this challenge, future work could explore the adoption of more advanced sequence-to-sequence models, such as Transformer [47] or Mamba [48], which are designed to handle variable-length sequences more efficiently. These models, with their ability to capture long-range dependencies and process sequences of arbitrary length, may further enhance the performance of deep learning techniques in PTA data analysis, pushing the boundaries of GW astronomy.

**Acknowledgments.**— This study is supported by the National Key Research and Development Program of China (Grant No. 2021YFC2201901, Grant No. 2021YFC2203004, Grant No. 2020YFC2200100 and Grant No. 2021YFC2201903). International Partnership Program of the Chinese Academy of Sciences, Grant No. 025GJHZ2023106GC. We also gratefully acknowledge the financial support from Brazilian agencies Fundação de Amparo à Pesquisa do Estado de São Paulo (FAPESP), Fundação de Amparo à Pesquisa do Estado do Rio Grande do Sul (FAPERGS), Fundação de Amparo à Pesquisa do Estado do Rio de Janeiro (FAPERJ), Conselho Nacional de Desenvolvimento Científico e Tecnológico (CNPq), and Coordenação de Aperfeiçoamento de Pessoal de Nível Superior (CAPES).

[1] M. A. McLaughlin, *Classical and Quantum Gravity* **30**, 224008 (2013).

[2] A. Brazier, S. Chatterjee, T. Cohen, J. M. Cordes, M. E. DeCesar, P. B. Demorest, J. S. Hazboun, M. T. Lam, R. S.

- Lynch, M. A. McLaughlin, et al., “The nanograv program for gravitational waves and fundamental physics,” (2019), [arXiv:1908.05356 \[astro-ph.IM\]](#).
- [3] R. D. Ferdman, R. van Haasteren, C. G. Bassa, M. Burgay, I. Cognard, A. Corongiu, N. D’amico, G. Desvignes, J. W. T. Hessels, G. H. Janssen, et al., *Classical and Quantum Gravity* **27**, 084014 (2010).
- [4] R. N. Manchester, G. B. Hobbs, M. Bailes, W. A. Coles, W. van Straten, M. J. Keith, R. M. Shannon, N. D. R. Bhat, A. J. Brown, S. Burke-Spolaor, et al., *Publications of the Astronomical Society of Australia* **30** (2006).
- [5] H. Xu, S. Chen, Y. Guo, J. Jiang, B. Wang, J. Xu, Z. Xue, R. N. Caballero, J. ping Yuan, Y. Xu, et al., *Research in Astronomy and Astrophysics* **23** (2023).
- [6] G. Agazie, A. Anumalapudi, A. M. Archibald, Z. Arzoumanian, P. T. Baker, B. Bécsy, L. Blecha, A. Brazier, P. R. Brook, S. Burke-Spolaor, et al., *The Astrophysical Journal Letters* **951** (2023).
- [7] J. Antoniadis, P. Arumugam, S. Arumugam, P. Auclair, S. Babak, M. Bagchi, A.-S. B. Nielsen, E. Barausse, C. G. Bassa, A. Bathula, et al., *Astronomy & Astrophysics* (2023).
- [8] A. Addazi, Y.-F. Cai, A. Marcianò, and L. Visinelli, *Phys. Rev. D* **109**, 015028 (2024).
- [9] S. R. Taylor, “The Nanohertz Gravitational Wave Astronomer,” (2021), [arXiv:2105.13270 \[astro-ph\]](#).
- [10] S. Babak, M. Falxa, G. Franciolini, and M. Pironi, *Phys. Rev. D* **110**, 063022 (2024).
- [11] R. Van Haasteren, Y. Levin, P. McDonald, and T. Lu, *Mon. Not. R. Astron. Soc.* **395**, 1005 (2009).
- [12] J. A. Ellis, M. Vallisneri, S. R. Taylor, and P. T. Baker, “Enterprise: Enhanced numerical toolbox enabling a robust pulsar inference suite,” Zenodo (2020).
- [13] J. Ellis and R. van Haasteren, “jellis18/ptmcmcsampler: Official release,” (2017).
- [14] S. R. Taylor and J. R. Gair, *Phys. Rev. D* **88**, 084001 (2013).
- [15] M. Falxa, J. Antoniadis, D. J. Champion, I. Cognard, G. Desvignes, L. Guillemot, H. Hu, G. Janssen, J. Jawor, R. Karuppusamy, et al., *Phys. Rev. D* **109**, 123010 (2024).
- [16] G. E. Freedman, A. D. Johnson, R. Van Haasteren, and S. J. Vigeland, *Phys. Rev. D* **107**, 043013 (2023).
- [17] R. Van Haasteren and M. Vallisneri, *Phys. Rev. D* **90**, 104012 (2014).
- [18] G. Hobbs, A. Archibald, Z. Arzoumanian, D. Backer, M. Bailes, N. D. R. Bhat, M. Burgay, S. Burke-Spolaor, D. Champion, I. Cognard, et al., *Class. Quantum Gravity* **27**, 084013 (2010).
- [19] M. Dax, S. R. Green, J. R. Gair, J. H. Macke, A. Buonanno, and B. Scholkopf, *Physical review letters* **127** **24**, 241103 (2021).
- [20] M. Dax, S. R. Green, J. R. Gair, M. Purrer, J. B. Wildberger, J. H. Macke, A. Buonanno, and B. Scholkopf, *Physical review letters* **130** **17**, 171403 (2022).
- [21] B. Liang, M. Du, H. Wang, Y. Xu, C. Liu, X. Wei, P. Xu, L. e Qiang, and Z. Luo, *Machine Learning: Science and Technology* **5**, 045040 (2024).
- [22] G. Papamakarios and I. Murray, “Fast  $\epsilon$ -free inference of simulation models with bayesian conditional density estimation,” (2018), [arXiv:1605.06376 \[stat.ML\]](#).
- [23] J.-M. Lueckmann, P. J. Goncalves, G. Bassetto, K. Öcal, M. Nonnenmacher, and J. H. Macke, “Flexible statistical inference for mechanistic models of neural dynamics,” (2017), [arXiv:1711.01861 \[stat.ML\]](#).
- [24] D. S. Greenberg, M. Nonnenmacher, and J. H. Macke, “Automatic posterior transformation for likelihood-free inference,” (2019), [arXiv:1905.07488 \[cs.LG\]](#).
- [25] M. Dax, J. B. Wildberger, S. Buchholz, S. R. Green, J. H. Macke, and B. Scholkopf, *ArXiv abs/2305.17161* (2023).
- [26] D. Shih, M. Freytsis, S. R. Taylor, J. A. Dror, and N. Smyth, *Physical review letters* **133** **1**, 011402 (2023).
- [27] M. Vallisneri, M. Crisostomi, A. D. Johnson, and P. M. Meyers, “Rapid parameter estimation for pulsar-timing-array datasets with variational inference and normalizing flows,” (2024), [arXiv:2405.08857 \[gr-qc\]](#).
- [28] R. w. Hellings and G. s. Downs, *Astrophys. J. Lett.* **265**, L39 (1983).
- [29] R. T. Q. Chen, Y. Rubanova, J. Bettencourt, and D. Duvenaud, “Neural ordinary differential equations,” (2019), [arXiv:1806.07366 \[cs.LG\]](#).
- [30] Y. Lipman, R. T. Q. Chen, H. Ben-Hamu, M. Nickel, and M. Le, “Flow matching for generative modeling,” (2023), [arXiv:2210.02747 \[cs.LG\]](#).
- [31] T. D. Gebhard, J. B. Wildberger, M. Dax, A. Kofler, D. Angerhausen, S. P. Quanz, and B. Scholkopf (2024).
- [32] Z. Arzoumanian, P. T. Baker, H. Blumer, B. Bécsy, A. Brazier, P. R. Brook, S. Burke-Spolaor, S. Chatterjee, S. Chen, J. M. Cordes, et al., *Astrophys. J. Lett.* **905**, L34 (2020).
- [33] C. P. Robert and W. Changye, “Markov chain monte carlo methods, a survey with some frequent misunderstandings,” (2020), [arXiv:2001.06249 \[stat.CO\]](#).
- [34] A. Tong, K. Fatras, N. Malkin, G. Hugué, Y. Zhang, J. Rector-Brooks, G. Wolf, and Y. Bengio, “Improving and generalizing flow-based generative models with minibatch optimal transport,” (2024), [arXiv:2302.00482 \[cs.LG\]](#).
- [35] P. Esser, S. Kulal, A. Blattmann, R. Entezari, J. Müller, H. Saini, Y. Levi, D. Lorenz, A. Sauer, F. Boesel, et al., “Scaling Rectified Flow Transformers for High-Resolution Image Synthesis,” (2024), [arXiv:2403.03206](#).
- [36] X. Liu, C. Gong, and Q. Liu, “Flow straight and fast: Learning to generate and transfer data with rectified flow,” (2022), [arXiv:2209.03003 \[cs.LG\]](#).
- [37] M. S. Albergo and E. Vanden-Eijnden, *ArXiv abs/2209.15571* (2022).
- [38] S. Hochreiter and J. Schmidhuber, *Neural Computation* **9**, 1735 (1997).
- [39] K. He, X. Zhang, S. Ren, and J. Sun, “Deep residual learning for image recognition,” (2015), [arXiv:1512.03385 \[cs.CV\]](#).
- [40] A. Paszke, S. Gross, F. Massa, A. Lerer, J. Bradbury, G. Chanan, T. Killeen, Z. Lin, N. Gimelshein, L. Antiga, et al., “Pytorch: An imperative style, high-performance deep learning library,” (2019), [arXiv:1912.01703 \[cs.LG\]](#).
- [41] C. R. Harris, K. J. Millman, S. J. van der Walt, R. Gommers, P. Virtanen, D. Cournapeau, E. Wieser, J. Taylor, S. Berg, N. J. Smith, et al., *Nature* **585**, 357 (2020).
- [42] F. Rozet et al., “Zuko: Normalizing flows in pytorch,” (2022).
- [43] F. Rozet, A. Delaunoy, B. Miller, et al., “LAMPE: Likelihood-free amortized posterior estimation,” (2021).
- [44] D. P. Kingma and J. Ba, “Adam: A method for stochastic optimization,” (2017), [arXiv:1412.6980 \[cs.LG\]](#).
- [45] P. Kidger, R. T. Q. Chen, and T. J. Lyons, *International Conference on Machine Learning* (2021).
- [46] R. T. Q. Chen, “torchdiffeq,” (2018).
- [47] A. Vaswani, N. Shazeer, N. Parmar, J. Uszkoreit, L. Jones, A. N. Gomez, Ł. Kaiser, and I. Polosukhin, in *Advances in Neural Information Processing Systems*, Vol. 30, edited

by I. Guyon, U. V. Luxburg, S. Bengio, H. Wallach,  
R. Fergus, S. Vishwanathan, and R. Garnett (Curran

Associates, Inc., 2017).  
[48] A. Gu and T. Dao, (2023), [arXiv:2312.00752 \[cs\]](#).